Draft version November 18, 2025
Typeset using LaTeX **twocolumn** style in AASTeX631

Orbital Eccentricities Suggest a Gradual Transition from Giant Planets to Brown Dwarfs

Gregory J. Gilbert,[1,2] Judah Van Zandt,[1,*] Erik A. Petigura,[1] Steven Giacalone,[2,†] Andrew W. Howard,[2] and Luke B. Handley[2]

[1] *Department of Physics & Astronomy, University of California Los Angeles, Los Angeles, CA 90095, USA*
[2] *Department of Astronomy, California Institute of Technology, Pasadena, CA 91125, USA*

ABSTRACT

To date, hundreds of sub-stellar objects with masses between $1 - 80\ M_{\rm Jup}$ have been detected orbiting main-sequence stars. The current convention uses the deuterium-burning limit, $M_c \approx 13 M_{\rm Jup}$ to divide this population between giant planets and brown dwarfs. However, this classification heuristic is largely divorced from any formation physics and may not accurately reflect the astrophysical nature of these objects. Previous work has suggested that a transition from "planet-like" to "brown-dwarf-like" characteristics occurs somewhere in the range $1 - 10 M_{\rm Jup}$, but precise the crossover mass and whether the transition is gradual or abrupt remains unknown. Here, we explore how the occurrence rate, host star metallicity, and orbital eccentricities vary as a function of mass in a sample of 70 Doppler-detected sub-stellar objects ($0.8 < M_c/M_{\rm Jup} < 80$) from the California Legacy Survey. Our population consists of objects near and beyond the water ice line ($1 < a/{\rm AU} < 10$), providing valuable clues to the details of giant planet formation physics at a location in the proto-stellar disk where planet formation efficiency is thought to be enhanced. We find that occurrence rate, host star metallicity, and orbital eccentricity all change gradually across the mass range under consideration, suggesting that "bottom-up" core accretion mechanisms and "top-down" gravitational instability mechanisms produce objects that overlap in mass. The observed eccentricity distributions could arise either from different formation channels or from post-formation dynamical interactions between massive sub-stellar objects.

1. INTRODUCTION

Astronomers have detected hundreds of sub-stellar objects with masses between $1 - 80\ M_{\rm Jup}$ orbiting main-sequence stars. Objects below this mass limit ($M_c < 1\ M_{\rm Jup}$) are classified as planets and are thought to form via rapid oligarchic growth of solid cores in the proto-stellar disk, followed by a period of runaway H/He gas accretion (J. B. Pollack et al. 1996). Objects above this mass limit ($M_c > 80\ M_{\rm Jup}$) form via direct gravitational collapse of molecular clouds and become main sequence stars which fuse hydrogen in their cores (e.g., C. F. McKee & E. C. Ostriker 2007). Objects in the intermediate regime ($M_c \approx 1{-}80\ M_{\rm Jup}$) may form through bottom-up core accretion (J. B. Pollack et al. 1996) or through top-down gravitational instability (A. P. Boss 1997). Historically, the deuterium-burning limit, $M_c \approx 13\ M_{\rm Jup}$ (D. S. Spiegel et al. 2011), has been used to divide the intermediate-mass population between giant planets and brown dwarfs. However, while deuterium burning can alter cooling rates and the age-luminosity relationship, its influence on bulk mass is far less pronounced (G. Chabrier et al. 2014). Furthermore, it is likely that the mass domains of the largest giant planets and the smallest brown dwarfs overlap considerably. Consequently, there exists an order-of-magnitude mass range over which sub-stellar objects cannot yet be unambiguously classified. The aim of this study is to clarify this distinction.

Numerous prior studies have sought to identify the transition from bottom-up formation to top-down formation on the basis of host star metallicity. Giant planets have long been known to form predominantly around high-metallicity stars (D. A. Fischer & J. Valenti 2005), a correlation that does not hold for small planets (L. A. Buchhave et al. 2012) or for high-mass brown dwarfs (B. Ma & J. Ge 2014). This correlation implies that enhanced disk metallicities are required for massive planetary cores to form and trigger runaway accretion prior to gas disk dispersal (S. Ida & D. N. C. Lin 2004). In contrast, gravitational instability has no such metallic-

Corresponding author: Gregory J. Gilbert
ggilbert@caltech.edu

* NASA FINESST Fellow

† NSF Astronomy and Astrophysics Postdoctoral Fellow

ity requirement (G. Chabrier et al. 2014). Using various populations of sub-stellar companions, some studies have identified a host star metallicity transition around $4-10\,M_{\rm Jup}$ (N. C. Santos et al. 2017; K. C. Schlaufman 2018; V. Adibekyan 2019), while others have identified a transition around $35-55\,M_{\rm Jup}$ (B. Ma & J. Ge 2014; D. Mata Sánchez et al. 2014; J. Maldonado & E. Villaver 2017). It is possible that the lower mass threshold corresponds to a transition from core accretion to disk instability, while the higher mass threshold corresponds to a transition from disk instability to direct fragmentation and gravitational collapse of the molecular cloud (A. K. Jappsen et al. 2005; D. Forgan & K. Rice 2011).

Orbital eccentricity provides a complementary and powerful probe of giant planet and brown dwarf formation physics. Studies of Doppler-detected, directly imaged, and transiting sub-stellar objects have consistently identified a qualitative trend wherein lower mass "planet-like" objects exhibit lower eccentricities compared to their higher mass "brown-dwarf-like" counterparts. Based on observations of 396 Doppler-detected giant planets (median $P = 382$ days), D. M. Kipping (2013) recovered an eccentricity distribution which was well-described by a beta distribution peaked at $e = 0$ with mean eccentricity $\langle e\rangle \approx 0.23$. In contrast, an analysis of Doppler-detected brown dwarf companions to FGK stars ($P \lesssim 2000$ days) by B. Ma & J. Ge (2014) observed a much more uniform distribution of eccentricities between $e \approx 0.0-0.9$. Similarly, B. P. Bowler et al. (2020) found that directly imaged giant planets ($M_p < 15\,M_{\rm Jup}$) at separations of 5–100 AU exhibit a preference for low eccentricities ($e \approx 0.05-0.25$), whereas their directly imaged brown dwarf counterparts ($M_p > 15\,M_{\rm Jup}$) possess a wide range of eccentricities peaked near $e \approx 0.6$. Although the exact values for the directly imaged population are somewhat sensitive to modeling choices (V. Nagpal et al. 2023; C. R. Do Ó et al. 2023), the broad conclusion that giant planets exhibit a narrow range of low eccentricities compared to a broad, high eccentricity distribution for brown dwarfs is robust. The trend toward low eccentricities for giant planets also holds true for close-in transiting planets ($P < 100$ days), which G. J. Gilbert et al. (2025) observed to possess a mean eccentricity $\langle e\rangle \approx 0.2$, consistent with both the intermediate-period Doppler-detected population (D. M. Kipping 2013) and the long-period directly-imaged population (B. P. Bowler et al. 2020). Thus, eccentricity measurements across a wide range of star-companion separations are all consistent with a paradigm whereby giant planets form by core accretion (S. Ida et al. 2013) and brown dwarfs form by gravitational instability (E. I. Vorobyov 2013; B. Ma & J. Ge 2014).

Here, we present evidence that the transition from planet-like objects to brown-dwarf-like objects near the ice line occurs gradually between $\sim 2-13 M_{\rm Jup}$. Our conclusion is based on a hierarchical Bayesian analysis of the orbital eccentricities of 70 Doppler-detected sub-stellar objects from the California Legacy Survey (CLS; L. J. Rosenthal et al. 2021). We combined CLS radial velocity measurements with *Hipparcos-Gaia* astrometry, thereby breaking the usual inclination degeneracy inherent to Doppler-only studies, allowing us to measure true mass M_c as opposed to minimum mass $M_c \sin i$. Leveraging the homogeneous search strategy employed by CLS, we corrected for survey completeness to recover the unbiased, intrinsic eccentricity distribution of objects between $0.8 - 80 M_{\rm Jup}$ at orbital separations between $1 - 10$ AU. Two companion papers to this study (Van Zandt et al., in review, Giacalone et al., in review) investigated the companion occurrence rates and host star metallicity properties of the CLS sample, reaching similar conclusions.

This paper is organized as follows. In §2 we review the California Legacy Survey. In §3 we describe our hierarchical analysis and discuss demographic trends in orbital eccentricities as a function of companion mass and separation. In §4 we discuss the astrophysical implications of our findings, and in §5 we summarize our conclusions.

2. OBSERVATIONS

2.1. *California-Legacy Survey radial velocities*

The California Legacy Survey (CLS; L. J. Rosenthal et al. 2021) monitored 719 bright, nearby stars taking over 100,000 precision radial velocity (RV) measurements using the Keck-HIRES, APF-Levy, and Lick-Hamilton spectrographs over more than thirty years. CLS recovered 226 companions, of which, by the classical dividing lines, 34 were stellar ($M \sin i > 80\ M_{\rm Jup}$), 19 were brown dwarfs ($13 < M \sin i / M_{\rm Jup} \leq 80$), and 173 — including 14 new discoveries — were planetary ($M \sin i \leq 13\ M_{\rm Jup}$). These detections spanned star-planet separations out to 20 AU and masses M_p down to $\sim 0.01\ M_{\rm Jup}$. In addition, CLS derived uniform properties for host stars using high-resolution spectral matching (`SpecMatch`; E. A. Petigura 2015; S. W. Yee et al. 2017) and isochrone fitting (`Isoclassify;` D. Huber 2017). The homogeneous observing strategy of CLS has made it a valuable resource for probing exoplanet demographics, particularly for planets at or near the water ice line (e.g. B. J. Fulton et al. 2021; J. Van Zandt & E. A. Petigura 2024).

For our present study, we chose to focus on the region of parameter space between $a = 1 - 10$ AU and $M_c = 0.8 - 80 M_{\rm Jup}$ (Figure 1). We chose this mass interval to cover Jovian planets, super-Jovians, and brown dwarfs, and we chose 1–10 AU in order to limit our analysis separations over which CLS had high sensitivity to companions and full orbital phase coverage. A total of 70 out of 226 companions reside in this mass-separation interval.

2.2. *Hipparcos-Gaia astrometry*

Doppler measurements alone provide only a minimum companion mass $M_c \sin i$ rather than a true mass M_c because radial velocities cannot constrain orbital inclination. To break this degeneracy and recover true masses, we combined CLS Doppler measurements with the *Hipparcos-Gaia* catalog of astrometric accelerations (HGCA; T. D. Brandt 2021). For a more detailed description of this procedure, see Van Zandt et al., in review. A summary is presented below.

HGCA provides astrometric proper motions for a catalog of over 115,000 stars, determined by aligning *Hipparcos* astrometric observations (Hip 1997) with those of *Gaia* EDR3 (L. Lindegren et al. 2021). By combining these astrometric accelerations with RV measurements, one may infer the presence of massive long-period planets and place separate constraints on M_c and $\sin i$.

We used `Orvara` (T. D. Brandt et al. 2021) to uniformly fit the orbits of the CLS systems hosting one or more companions with $M \sin i \leq 80\ M_{\rm Jup}$. We fit three-dimensional orbits, including inclination i and longitude of the ascending node Ω, with the aim of constraining companion true mass M_c rather than $M_c \sin i$. We used the RV measurements provided in L. J. Rosenthal et al. (2021) for all systems, and we incorporated HGCA astrometric accelerations for the 53 systems in which the acceleration was significant ($\Delta\mu/\sigma(\Delta\mu) \geq 3$). For the remaining 75 systems, we supplied no astrometric data and fit only the RVs, allowing `Orvara` to marginalize over the uncertainty in inclination.

3. ECCENTRICITY ANALYSIS

3.1. *Survey completeness*

The primary goal of CLS was to measure planet occurrence rates, a task which demands careful appraisal of search completeness. As such, L. J. Rosenthal et al. (2021) measured CLS system-by-system sensitivity to planetary, sub-stellar, and stellar companions through a suite of injection-and-recovery tests. These tests were performed by randomly drawing a set of orbital parameters (P, t_p, e, ω, K), forward-modeling the RV signature that a companion with those parameters would produce, injecting that signature into a system's actual RV time series to capture system-specific RV noise and sampling inhomogeneities, and attempting to recover the signal with a signal detection pipeline. L. J. Rosenthal et al. (2021) repeated this procedure 1000 times for each system, and estimated sensitivity as the fraction of successful recoveries in a given region of M_p–a space. This procedure facilitated high-confidence measurement of giant planet occurrence near the ice line (B. J. Fulton et al. 2021) and the conditional occurrence rate of these giant planets in the presence of close-in small planets ($M_p = 2 - 30 M_\oplus, a < 1$AU; L. J. Rosenthal et al. 2022).

CLS injection-and-recovery tests assumed a beta distribution for eccentricity and marginalized over e in their completeness maps. This procedure was adequate to determine occurrence rates, but may still introduce subtle biases to the inferred eccentricity distribution of the population. So, to more thoroughly explore the role of eccentricity in survey completeness, we retrieved the original injection-and-recovery results calculated by L. J. Rosenthal et al. (2021) and divided them into bins according to eccentricity ($e = 0.0 - 0.9, \Delta e = 0.1$). For each discrete value of e, we computed a completeness map following established procedures that treat occurrence as a censored Poisson point process (D. Foreman-Mackey et al. 2014; B. J. Fulton et al. 2021; J. Van Zandt & E. A. Petigura 2024, Van Zandt et al., in review). Finally, we interpolated these completeness maps to determine detection efficiency $\hat{d}_{nk}$ for each of the $\{M_c, a, e\}_{nk}$ samples returned by our joint RV-astrometry fits.

3.2. *Hierarchical population inference*

By eye, there is a clear trend of rising eccentricity with increasing companion mass (Figure 2). To precisely quantify this trend, we adopt the approximate hierarchical Bayesian modeling framework used by G. J. Gilbert et al. (2025) to infer the eccentricity distribution of transiting planets. Our procedure builds upon the formalism originally described by D. W. Hogg et al. (2010) and further developed by D. Foreman-Mackey et al. (2014), V. Van Eylen et al. (2019), and K. Masuda et al. (2022). A summary of our procedure is as follows.

Our joint RV–astrometry fits for N planets each produced a set of K posterior eccentricity samples e_{nk}. For the majority of targets, eccentricity values were tightly constrained, with $\sigma(e) \lesssim 0.1$. The combined likelihood for the population eccentricity distribution $f(e)$ is

$$\mathcal{L}(e;\alpha) = \prod_{n=1}^{N} \frac{1}{K} \sum_{k=1}^{K} \frac{f(e_{nk};\alpha)}{p_0(e_{nk})} \hat{d}(e_{nk}), \tag{1}$$

where $p_0(e)$ is the uninformative "interim" prior on e applied during model fitting and $f(e;\alpha)$ is the informa-

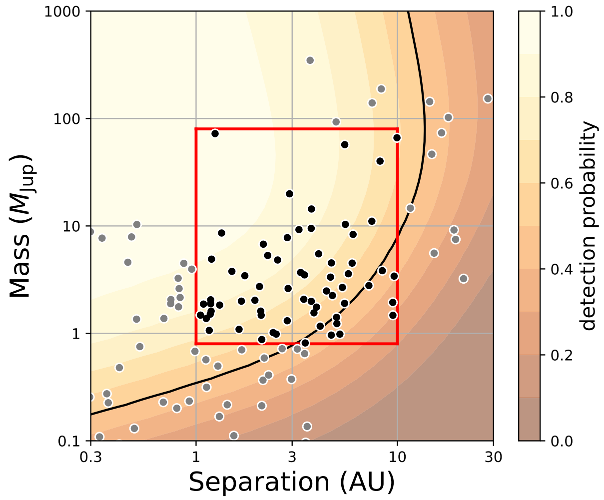

Figure 1. Masses and orbital separations of the sub-stellar companions detected by CLS. Black points indicate objects included in our study, whereas gray points are shown for context but not included in our analysis. The colored contours indicate the detection probability for a sub-stellar companion with a given mass and orbital separation and a nominal eccentricity $e = 0.2$. The black contour shows the 50% sensitivity line. The red rectangle indicates our chosen parameter space for this study, where completeness is high.

tive "updated" population distribution we wish to infer. For our purposes, $p_0(e) = 1$, since e was sampled assuming a uniform prior. The quantity α is the vector of hyper-parameters describing the updated population distribution, and $\hat{d}(e_{nk})$ weights the samples to account for detection completeness (see §3.1 and Van Zandt et al., in review). We performed the analysis both with and without including this completeness correction and found it made virtually no difference in the inferred eccentricity distributions. Such insensitivity to completeness corrections is unsurprising, as we chose this region intentionally for its high completeness.

Following G. J. Gilbert et al. (2025), we adopted a flexible non-parametric model for $f(e; \alpha)$ which describes the eccentricity distribution as a regularized histogram. The advantage of using a regularized histogram is that it makes no assumptions about the shape or functional form of the distribution other than requiring that the distribution be smooth and continuous.

For a histogram with M bins, the function is defined as

$$f(e; \alpha) = \sum_{m=1}^{M} \exp(\alpha_m)\gamma(e; a_m, b_m) \tag{2}$$

where the hyper-parameters $\{\alpha_m\}$ are the logarithmic bin heights, $\{a_m, b_m\}$ define the fixed locations of the histogram bin edges such that each of the bins has width $\Delta e_m = b_m - a_m$, and $\gamma(e)$ is a correction factor

$$\gamma(e; a, b) = \begin{cases} \frac{1}{b-a}, & \text{if } a \le e < b \\ 0, & \text{otherwise} \end{cases} \tag{3}$$

which accounts for the finite bin widths.

To ensure proper normalization of the probability density function $f(e)$ we transformed α_m via

$$\alpha'_m = \alpha_m - \ln\left(\sum_{m=1}^{M} \exp(\alpha_m)\Delta e_m\right) \tag{4}$$

so that $\sum_m \exp(\alpha'_m)\Delta e_m = 1$. We used 40 bins, so each bin had a width $\Delta e_m = 0.025$.

We enforced smoothness in the histogram by applying a Gaussian Process (GP) prior on α using a Matérn-3/2 kernel. The covariance function of this kernel is

$$\kappa(e) = s^2\left(1 + \frac{\sqrt{3}e}{\ell}\right)\exp\left(-\frac{\sqrt{3}e}{\ell}\right) \tag{5}$$

where s sets the scale and ℓ sets the correlation length. In practice, we achieved good results by applying a modestly informative log-normal hyper-priors on the GP hyperparameters $\ln(s) \sim \mathcal{N}(3, 1)$ and $\ln(\ell) \sim \mathcal{N}(0, 1)$. These hyper-priors prevented the sampler from wandering too far from the maximum likelihood region of parameter space and enforced a certain degree of smoothness in the distribution. Latent bin heights α were drawn from a standard normal distribution and scaled according to the GP prior.

To determine the relationship between M_c and $f(e)$, we split the sub-stellar object population into five approximately log-uniform mass bins, with bin edges at $M_c/M_{\rm Jup} = [0.8, 1.6, 3.2, 6.5, 13, 80]$; the larger bin size for classical brown dwarfs was chosen to accommodate the small sample size for these objects. To maximize information content, Gaussian process regularization hyperparameters $\{s, \ell\}$ were shared between the five groups, which is equivalent to assuming that the various sub-populations have eccentricity distributions with roughly comparable smoothness. Other than this mild assumption, no further relationship between the sub-populations was imposed. We sampled from the posterior using `PyMC3` and a gradient-based Hamiltonian Monte Carlo implementation of the No U-Turn Sampling (NUTS) algorithm (M. D. Hoffman & A. Gelman 2011; M. J. Betancourt & M. Girolami 2013; J. Salvatier et al. 2015). Our fitting algorithm produced posterior samples for the intrinsic distribution $f(e)$ for each of the five sub-populations.

Eccentricities for individual objects and sub-populations binned by sub-stellar object mass are shown in Figure 2. From the raw data alone (left panel), we observed a clear trend of rising eccentricity with rising mass, with objects below $M = 1.6 M_{\rm Jup}$ preferring $e \lesssim 0.5$ and objects above $M = 13 M_{\rm Jup}$ preferring $e \gtrsim 0.2$. Our hierarchical inference (right panel) further revealed that there is a smooth transition in the mean eccentricity $\langle e \rangle$ and the overall shape of the distribution from the lowest mass bin to the highest mass bin). Furthermore, the relationship between M_c and e appears to be monotonic. The distribution the lowest mass bin is peaked at $e = 0$ and falls quasi-exponentially toward zero at $e = 1$, transitioning gradually toward a nearly uniform distribution for the nominal deuterium-burning brown dwarfs.

4. DISCUSSION

Our hierarchical inference of population eccentricity distributions suggests that the transition from low-mass, low-eccentricity objects to high-mass, varied-eccentricity objects is gradual between $1 - 10 M_{\rm Jup}$. This positive correlation between M_c and $\langle e \rangle$ is expected from theoretical models of strong gravitational scattering, and does not necessarily indicate that the higher mass objects formed in a qualitatively distinct manner from the lower mass objects. (S. Chatterjee et al. 2008; E. B. Ford & F. A. Rasio 2008; M. Jurić & S. Tremaine 2008; S. Ida et al. 2013). Moreover, no apparent upper limit on eccentricities that may be formed by planet-planet scattering, although proto-planetary architectures which produce $e \gtrsim 0.8$ via gravitational scattering are rare (D. Carrera et al. 2019).

To place our new eccentricity measurements in context, we consider each sub-population's mean eccentricity $\langle e \rangle$ alongside host star metallicity [Fe/H] and companion occurrence rate density (see Figure 3). We found that whereas occurrence rate density steadily decreases with increasing M_c (Van Zandt et al., in review), [Fe/H] and M_c exhibit no strong relationship for our sample.

The observed anti-correlation between occurrence rate density and M_c is consistent with previous analyses which found a paucity of brown dwarfs inside $a \lesssim 3$ AU (i.e. the so-called "Brown Dwarf desert"; D. Grether & C. H. Lineweaver 2006). The lack of a correlation between [Fe/H] and M_c, however, stands in tension with previous studies which have claimed to identify a transition in host star metallicity and M_c between $4 - 10 M_{\rm Jup}$ (N. C. Santos et al. 2017; K. C. Schlaufman 2018; V. Adibekyan 2019). Nevertheless, we caution against over-interpreting this tension, as the comparison is not strictly one-to-one. For example, K. C. Schlaufman (2018) placed the metallicity-derived dividing line at $M_c \approx 4 M_{\rm Jup}$, grouping objects between $0.2 < M_c/M_{\rm Jup} < 4$ vs $4 < M_c/M_{\rm Jup} < 300$, meaning their analysis included smaller planets in the first group and both large brown dwarfs and very low mass stars in the second group. In addition, these previous analyses focused on samples of close-in objects, whereas our sample extends out to 10 AU, near the orbit of Saturn. A companion study to this work, Giacalone et al. (in review) places the transition at $M_c = 25^{+9}_{-7} M_{\rm Jup}$ for the CLS sample, with a broad range of permissible values (95% confidence interval [14,48] $M_{\rm Jup}$). So, our non-detection of a threshold mass below $13 M_{\rm Jup}$ where host star [Fe/H] abruptly changes is not an outright contraction.

The lack of a sharp transition in occurrence, host star metallicity, and orbital eccentricity between giant planets and brown dwarfs is qualitatively different than the sharp transition in these quantities between small planets ($R_p < 3.5 R_\oplus$) and large planets ($R_p > 3.5 R_\oplus$) found by G. J. Gilbert et al. (2025). Whereas giant planet formation appears to be a threshold process — i.e. an "all-or-nothing" event predicated on whether a protoplanetary core reaches the requisite mass for runaway H/He envelope accretion (J. B. Pollack et al. 1996) — there appears to be no such threshold governing whether or if a super-giant planet turns into a brown dwarf. The simplest explanation for our non-detection of a sharp threshold is that both bottom-up and top-down formation mechanisms produce objects in the range $1 - 10 M_{\rm Jup}$. Exactly how large of an object can be formed by core accretion or how small of an object can be formed by disk instability or cloud fragmentation remains to be determined. Nevertheless, theoretical models suggest that sub-stellar companions with masses $M_c \sim 10 M_{\rm Jup}$ can be formed under rare but feasible circumstances via both bottom-up (H. Tanaka et al. 2020) and top-down channels (D. Stamatellos et al. 2007; S. E. Dodson-Robinson et al. 2009; A. P. Boss 2011; E. I. Vorobyov & V. G. Elbakyan 2018). So, we may reasonably assume that as the mass of an object increases, the likelihood that it formed via core accretion drops and the likelihood that it formed by gravitational instability rises.

5. CONCLUSION

We analyzed the eccentricities of 70 sub-stellar objects with masses between $0.8 - 80 M_{\rm Jup}$ using a hierarchical Bayesian framework. These objects were uniformly detected and vetted by the California Legacy Survey (CLS), enabling completeness corrections and unbiased population inference. Our main conclusions are as follows.

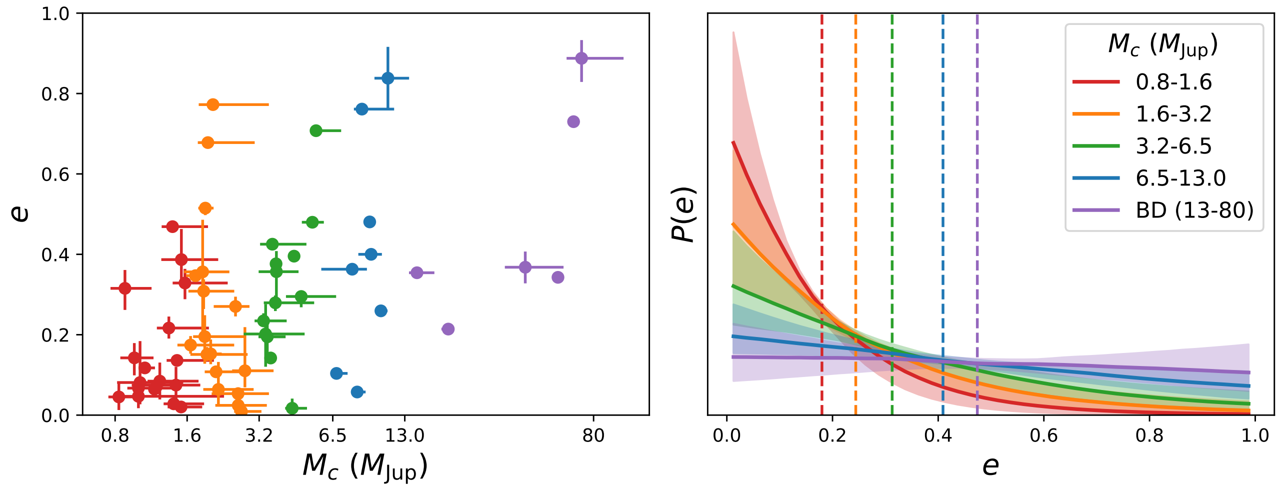

Figure 2. The eccentricities of sub-stellar objects with star-companion orbital separations $a = 1 - 10$AU and true masses $M_c = 0.8 - 80M_{\rm Jup}$. *Left panel*: Mass vs. eccentricity. Colors correspond to our nominal size bins. There is a clear trend of rising eccentricity with rising mass, with objects below $M = 1.6M_{\rm Jup}$ preferring $e \lesssim 0.5$ and objects above $M = 13M_{\rm Jup}$ preferring $e \gtrsim 0.2$. *Right panel*: Sub-population eccentricity distributions inferred using a hierarchical Bayesian model. Solid lines indicate the median posterior distribution, shaded regions indicate 1σ confidence intervals, and dashed lines indicated the mean for each subpopulation. There is a smooth transition in the mean eccentricity $\langle e \rangle$ and the overall shape of the distribution from the lowest mass bin (peaked at $e = 0$ and monotonically declining toward zero at $e = 1$) to the highest pass bin (nearly uniform over e).

- Doppler-detected Jovian-mass objects between 1–10 AU have $\langle e \rangle \approx 0.2$ whereas brown dwarfs above the deuterium burning limit have $\langle e \rangle \approx 0.5$.
- The transition in $\langle e \rangle$ and $f(e)$ from low-mass to high-mass objects is gradual over this mass range.
- Changes in host star metallicity and companion occurrence rates are also gradual in this regime. These trends imply that bottom-up formation mechanisms (i.e. core accretion) and top-down mechanisms (i.e. gravitational instability) produce sub-stellar objects that overlap in mass.

Our results are consistent with numerous previous analyses which demonstrated that giant planets tend to have low eccentricities with a relatively narrow spread in values (D. M. Kipping 2013; B. P. Bowler et al. 2020; G. J. Gilbert et al. 2025), whereas brown dwarfs tend to have a more nearly uniform distribution of eccentricities (B. Ma & J. Ge 2014; B. P. Bowler et al. 2020). By focusing on a relatively narrow region of parameter space ($a = 1 - 10$ AU, $M_c = 0.8 - 80M_{\rm Jup}$), we demonstrated that the transition between the giant planet regime and the brown dwarf regime is gradual, with slow-and-steady changes not only in eccentricity, but also in occurrence rate and metallicity (see Van Zandt et al., in review and Giacalone et al, in review for further discussion).

This project endeavored to identify a dynamical signature that could be used to distinguish super-giant planets from small brown dwarfs.

Unfortunately, it appears that eccentricity alone does not provide sufficient information. Perhaps a clean dividing line between formation channels does exist, but we have not yet found it either because we do not have enough objects or because we have not yet examined the right combination of parameters. Recall, for example, how much cleaner the "radius gap" separating super-Earths and sub-Neptunes appears in the 2D space of period and radius rather than the 1D space of radius alone (B. J. Fulton et al. 2017; B. J. Fulton & E. A. Petigura 2018). For giant planets and brown dwarfs, perhaps one could fold together other quantities such as star-companion spin-orbit angle, companion spin rate, companion atmospheric chemistry or other quantities alongside mass and eccentricity to find a clean separation between top-down vs bottom-up channels.

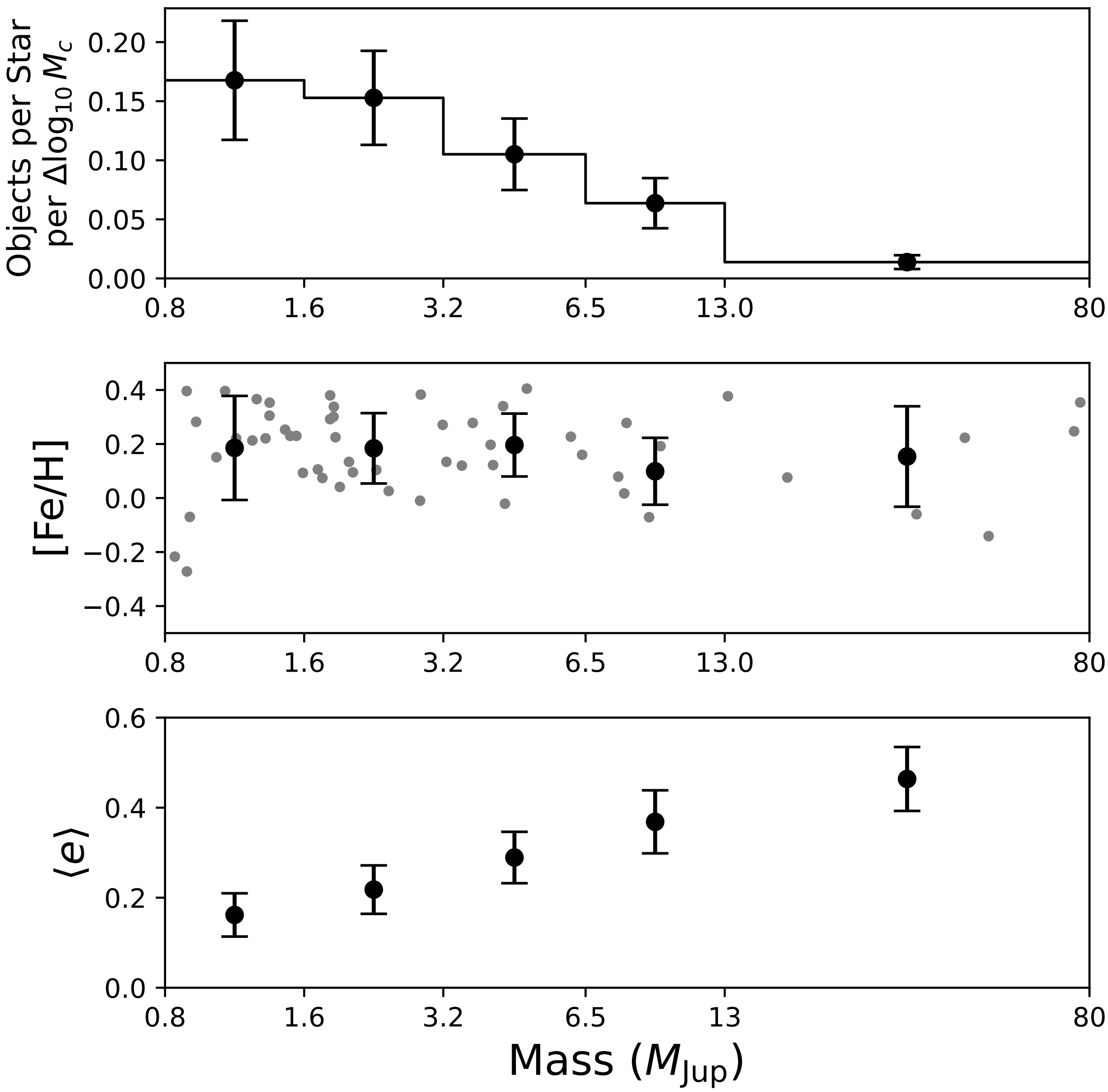

Figure 3. Demographic trends in occurrence rate density, host star metallicity, and orbital eccentricity for sub-stellar objects between $0.8 - 80 M_{\rm Jup}$. All three demographic trends display a smooth variation with companion mass. *Top panel*: Occurrence rate per logarithmic mass bin falls steadily as M_c increases. *Middle panel*: The relationship between host star metallicity and companion mass is weak-to-nonexistent, but may be weakly anti-correlated. *Bottom panel*: Mean eccentricity $\langle e \rangle$ rises steadily as M_c increases.

ACKNOWLEDGMENTS

We thank the anonymous referee for helpful comments which improved the quality of the manuscript. We are grateful for insightful conversations with Erik Ford and Ruth Murray-Clay which guided the interpretation of results.

Funding for this work was provided by a University of California, Los Angeles set-up award to E.A.P. and by the Heising-Simons Foundation Award 2022-3833. J.V.Z. was supported by NASA FINESST Fellowship 80NSSC22K1606.

This research has made use of the NASA Exoplanet Archive, which is operated by the California Institute of Technology, under contract with the National Aeronautics and Space Administration under the Exoplanet Exploration Program. This research has made use of the Astrophysics Data System, funded by NASA under Cooperative Agreement 80NSSC25M7105.

Some of the data presented herein were obtained at Keck Observatory, which is a private 501(c)3 non-profit organization operated as a scientific partnership among the California Institute of Technology, the University of California, and the National Aeronautics and Space Administration. The Observatory was made possible by the generous financial support of the W. M. Keck Foundation.

The authors wish to recognize and acknowledge the very significant cultural role and reverence that the summit of Maunakea has always had within the Native Hawaiian community. We are most fortunate to have the opportunity to conduct observations from this mountain.

Software: `astropy` (Astropy Collaboration et al. 2018), `numpy` (C. R. Harris et al. 2020), `scipy` (P. Virtanen et al. 2020), `pymc3` (J. Salvatier et al. 2015)

REFERENCES

1997, ESA Special Publication, Vol. 1200, The HIPPARCOS and TYCHO catalogues. Astrometric and photometric star catalogues derived from the ESA HIPPARCOS Space Astrometry Mission

Adibekyan, V. 2019, Heavy Metal Rules. I. Exoplanet Incidence and Metallicity, Geosciences, 9, 105, doi: 10.3390/geosciences9030105

Astropy Collaboration, Price-Whelan, A. M., Sipőcz, B. M., et al. 2018, The Astropy Project: Building an Open-science Project and Status of the v2.0 Core Package, AJ, 156, 123, doi: 10.3847/1538-3881/aabc4f

Betancourt, M. J., & Girolami, M. 2013, Hamiltonian Monte Carlo for Hierarchical Models, arXiv e-prints, arXiv:1312.0906, doi: 10.48550/arXiv.1312.0906

Boss, A. P. 1997, Giant planet formation by gravitational instability., Science, 276, 1836, doi: 10.1126/science.276.5320.1836

Boss, A. P. 2011, Formation of Giant Planets by Disk Instability on Wide Orbits Around Protostars with Varied Masses, ApJ, 731, 74, doi: 10.1088/0004-637X/731/1/74

Bowler, B. P., Blunt, S. C., & Nielsen, E. L. 2020, Population-level Eccentricity Distributions of Imaged Exoplanets and Brown Dwarf Companions: Dynamical Evidence for Distinct Formation Channels, AJ, 159, 63, doi: 10.3847/1538-3881/ab5b11

Brandt, T. D. 2021, The Hipparcos-Gaia Catalog of Accelerations: Gaia EDR3 Edition, ApJS, 254, 42, doi: 10.3847/1538-4365/abf93c

Brandt, T. D., Dupuy, T. J., Li, Y., et al. 2021, orvara: An Efficient Code to Fit Orbits Using Radial Velocity, Absolute, and/or Relative Astrometry, AJ, 162, 186, doi: 10.3847/1538-3881/ac042e

Buchhave, L. A., Latham, D. W., Johansen, A., et al. 2012, An abundance of small exoplanets around stars with a wide range of metallicities, Nature, 486, 375, doi: 10.1038/nature11121

Carrera, D., Raymond, S. N., & Davies, M. B. 2019, Planet-planet scattering as the source of the highest eccentricity exoplanets, A&A, 629, L7, doi: 10.1051/0004-6361/201935744

Chabrier, G., Johansen, A., Janson, M., & Rafikov, R. 2014, in Protostars and Planets VI, ed. H. Beuther, R. S. Klessen, C. P. Dullemond, & T. Henning, 619–642, doi: 10.2458/azu_uapress_9780816531240-ch027

Chatterjee, S., Ford, E. B., Matsumura, S., & Rasio, F. A. 2008, Dynamical Outcomes of Planet-Planet Scattering, ApJ, 686, 580, doi: 10.1086/590227

Do Ó, C. R., O'Neil, K. K., Konopacky, Q. M., et al. 2023, The Orbital Eccentricities of Directly Imaged Companions Using Observable-based Priors: Implications for Population-level Distributions, AJ, 166, 48, doi: 10.3847/1538-3881/acdc9a

Dodson-Robinson, S. E., Veras, D., Ford, E. B., & Beichman, C. A. 2009, The Formation Mechanism of Gas Giants on Wide Orbits, ApJ, 707, 79, doi: 10.1088/0004-637X/707/1/79

Fischer, D. A., & Valenti, J. 2005, The Planet-Metallicity Correlation, ApJ, 622, 1102, doi: 10.1086/428383

Ford, E. B., & Rasio, F. A. 2008, Origins of Eccentric Extrasolar Planets: Testing the Planet-Planet Scattering Model, ApJ, 686, 621, doi: 10.1086/590926

Foreman-Mackey, D., Hogg, D. W., & Morton, T. D. 2014, Exoplanet Population Inference and the Abundance of Earth Analogs from Noisy, Incomplete Catalogs, ApJ, 795, 64, doi: 10.1088/0004-637X/795/1/64

Forgan, D., & Rice, K. 2011, The Jeans mass as a fundamental measure of self-gravitating disc fragmentation and initial fragment mass, MNRAS, 417, 1928, doi: 10.1111/j.1365-2966.2011.19380.x

Fulton, B. J., & Petigura, E. A. 2018, The California-Kepler Survey. VII. Precise Planet Radii Leveraging Gaia DR2 Reveal the Stellar Mass Dependence of the Planet Radius Gap, AJ, 156, 264, doi: 10.3847/1538-3881/aae828

Fulton, B. J., Petigura, E. A., Howard, A. W., et al. 2017, The California-Kepler Survey. III. A Gap in the Radius Distribution of Small Planets, AJ, 154, 109, doi: 10.3847/1538-3881/aa80eb

Fulton, B. J., Rosenthal, L. J., Hirsch, L. A., et al. 2021, California Legacy Survey. II. Occurrence of Giant Planets beyond the Ice Line, ApJS, 255, 14, doi: 10.3847/1538-4365/abfcc1

Gilbert, G. J., Petigura, E. A., & Entrican, P. M. 2025, Planets larger than Neptune have elevated eccentricities, Proceedings of the National Academy of Science, 122, e2405295122, doi: 10.1073/pnas.2405295122

Grether, D., & Lineweaver, C. H. 2006, How Dry is the Brown Dwarf Desert? Quantifying the Relative Number of Planets, Brown Dwarfs, and Stellar Companions around Nearby Sun-like Stars, ApJ, 640, 1051, doi: 10.1086/500161

Harris, C. R., Millman, K. J., van der Walt, S. J., et al. 2020, Array programming with NumPy, Nature, 585, 357–362, doi: 10.1038/s41586-020-2649-2

Hoffman, M. D., & Gelman, A. 2011, The No-U-Turn Sampler: Adaptively Setting Path Lengths in Hamiltonian Monte Carlo, arXiv e-prints, arXiv:1111.4246, doi: 10.48550/arXiv.1111.4246

Hogg, D. W., Myers, A. D., & Bovy, J. 2010, Inferring the Eccentricity Distribution, ApJ, 725, 2166, doi: 10.1088/0004-637X/725/2/2166

Huber, D. 2017, isoclassify: v1.2,, v1.2 Zenodo, doi: 10.5281/zenodo.573372

Ida, S., & Lin, D. N. C. 2004, Toward a Deterministic Model of Planetary Formation. II. The Formation and Retention of Gas Giant Planets around Stars with a Range of Metallicities, ApJ, 616, 567, doi: 10.1086/424830

Ida, S., Lin, D. N. C., & Nagasawa, M. 2013, Toward a Deterministic Model of Planetary Formation. VII. Eccentricity Distribution of Gas Giants, ApJ, 775, 42, doi: 10.1088/0004-637X/775/1/42

Jappsen, A. K., Klessen, R. S., Larson, R. B., Li, Y., & Mac Low, M. M. 2005, The stellar mass spectrum from non-isothermal gravoturbulent fragmentation, A&A, 435, 611, doi: 10.1051/0004-6361:20042178

Jurić, M., & Tremaine, S. 2008, Dynamical Origin of Extrasolar Planet Eccentricity Distribution, ApJ, 686, 603, doi: 10.1086/590047

Kipping, D. M. 2013, Parametrizing the exoplanet eccentricity distribution with the beta distribution., MNRAS, 434, L51, doi: 10.1093/mnrasl/slt075

Lindegren, L., Klioner, S. A., Hernández, J., et al. 2021, Gaia Early Data Release 3. The astrometric solution, A&A, 649, A2, doi: 10.1051/0004-6361/202039709

Ma, B., & Ge, J. 2014, Statistical properties of brown dwarf companions: implications for different formation mechanisms, MNRAS, 439, 2781, doi: 10.1093/mnras/stu134

Maldonado, J., & Villaver, E. 2017, Searching for chemical signatures of brown dwarf formation, A&A, 602, A38, doi: 10.1051/0004-6361/201630120

Masuda, K., Petigura, E. A., & Hall, O. J. 2022, Inferring the rotation period distribution of stars from their projected rotation velocities and radii: Application to late-F/early-G Kepler stars, MNRAS, 510, 5623, doi: 10.1093/mnras/stab3650

Mata Sánchez, D., González Hernández, J. I., Israelian, G., et al. 2014, Chemical abundances of stars with brown-dwarf companions, A&A, 566, A83, doi: 10.1051/0004-6361/201423803

McKee, C. F., & Ostriker, E. C. 2007, Theory of Star Formation, ARA&A, 45, 565, doi: 10.1146/annurev.astro.45.051806.110602

Nagpal, V., Blunt, S., Bowler, B. P., et al. 2023, The Impact of Bayesian Hyperpriors on the Population-level Eccentricity Distribution of Imaged Planets, AJ, 165, 32, doi: 10.3847/1538-3881/ac9fd2

Petigura, E. A. 2015, PhD thesis, University of California, Berkeley

Pollack, J. B., Hubickyj, O., Bodenheimer, P., et al. 1996, Formation of the Giant Planets by Concurrent Accretion of Solids and Gas, Icarus, 124, 62, doi: 10.1006/icar.1996.0190

Rosenthal, L. J., Fulton, B. J., Hirsch, L. A., et al. 2021, The California Legacy Survey. I. A Catalog of 178 Planets from Precision Radial Velocity Monitoring of 719 Nearby Stars over Three Decades, ApJS, 255, 8, doi: 10.3847/1538-4365/abe23c

Rosenthal, L. J., Knutson, H. A., Chachan, Y., et al. 2022, The California Legacy Survey. III. On the Shoulders of (Some) Giants: The Relationship between Inner Small Planets and Outer Massive Planets, ApJS, 262, 1, doi: 10.3847/1538-4365/ac7230

Salvatier, J., Wiecki, T., & Fonnesbeck, C. 2015, Probabilistic Programming in Python using PyMC, arXiv e-prints, arXiv:1507.08050, doi: 10.48550/arXiv.1507.08050

Santos, N. C., Adibekyan, V., Figueira, P., et al. 2017, Observational evidence for two distinct giant planet populations, A&A, 603, A30, doi: 10.1051/0004-6361/201730761

Schlaufman, K. C. 2018, Evidence of an Upper Bound on the Masses of Planets and Its Implications for Giant Planet Formation, ApJ, 853, 37, doi: 10.3847/1538-4357/aa961c

Spiegel, D. S., Burrows, A., & Milsom, J. A. 2011, The Deuterium-burning Mass Limit for Brown Dwarfs and Giant Planets, ApJ, 727, 57, doi: 10.1088/0004-637X/727/1/57

Stamatellos, D., Hubber, D. A., & Whitworth, A. P. 2007, Brown dwarf formation by gravitational fragmentation of massive, extended protostellar discs, MNRAS, 382, L30, doi: 10.1111/j.1745-3933.2007.00383.x

Tanaka, H., Murase, K., & Tanigawa, T. 2020, Final Masses of Giant Planets. III. Effect of Photoevaporation and a New Planetary Migration Model, ApJ, 891, 143, doi: 10.3847/1538-4357/ab77af

Van Eylen, V., Albrecht, S., Huang, X., et al. 2019, The Orbital Eccentricity of Small Planet Systems, AJ, 157, 61, doi: 10.3847/1538-3881/aaf22f

Van Zandt, J., & Petigura, E. A. 2024, No Evidence for a Metallicity-dependent Enhancement of Distant Giant Companions to Close-in Small Planets in the California Legacy Survey, AJ, 168, 268, doi: 10.3847/1538-3881/ad8c3b10.1134/S1063772908070056

Virtanen, P., Gommers, R., Oliphant, T. E., et al. 2020, SciPy 1.0: Fundamental Algorithms for Scientific Computing in Python, Nature Methods, 17, 261, doi: 10.1038/s41592-019-0686-2

Vorobyov, E. I. 2013, Formation of giant planets and brown dwarfs on wide orbits, A&A, 552, A129, doi: 10.1051/0004-6361/201220601

Vorobyov, E. I., & Elbakyan, V. G. 2018, Gravitational fragmentation and formation of giant protoplanets on orbits of tens of au, A&A, 618, A7, doi: 10.1051/0004-6361/201833226

Yee, S. W., Petigura, E. A., & von Braun, K. 2017, Precision Stellar Characterization of FGKM Stars using an Empirical Spectral Library, ApJ, 836, 77, doi: 10.3847/1538-4357/836/1/77